Naval Research Laboratory
Washington, DC 20375-5000

NRL Memorandum Report 6286

X-Ray Spectroscopy of Laser-Produced L-Series Lines

P. G. BURKHALTER AND D. A. NEWMAN*

Condensed Matter Physics Branch
Condensed Matter and Radiation Sciences Division

**Sachs/Freeman Assoicates*
Landover, MD

August 31 1988

SECURITY CLASSIFICATION OF THIS PAGE

REPORT DOCUMENTATION PAGE

Form Approved
OMB No 0704-0188

1a REPORT SECURITY CLASSIFICATION UNCLASSIFIED	1b RESTRICTIVE MARKINGS
2a SECURITY CLASSIFICATION AUTHORITY	3 DISTRIBUTION / AVAILABILITY OF REPORT Approved for public release; distribution unlimited.
2b DECLASSIFICATION / DOWNGRADING SCHEDULE	
4 PERFORMING ORGANIZATION REPORT NUMBER(S) NRL Memorandum Report 6286	5 MONITORING ORGANIZATION REPORT NUMBER(S)
6a NAME OF PERFORMING ORGANIZATION Naval Research Laboratory 6b OFFICE SYMBOL (If applicable) Code 4681	7a NAME OF MONITORING ORGANIZATION
6c ADDRESS (City, State, and ZIP Code) Washington, DC 20375-5000	7b ADDRESS (City, State, and ZIP Code)
8a NAME OF FUNDING / SPONSORING ORGANIZATION Department of Energy 8b OFFICE SYMBOL (If applicable)	9 PROCUREMENT INSTRUMENT IDENTIFICATION NUMBER
8c ADDRESS (City, State, and ZIP Code) Washington, DC	10 SOURCE OF FUNDING NUMBERS PROGRAM ELEMENT NO: 81802 / PROJECT NO / TASK NO / WORK UNIT ACCESSION NO

11 TITLE (Include Security Classification)
X-Ray Spectroscopy of Laser-Produced L-Series Lines

12 PERSONAL AUTHOR(S)
Burkhalter, P.G. and Newman,* D.A.

13a TYPE OF REPORT	13b TIME COVERED	14 DATE OF REPORT (Year, Month, Day)	15 PAGE COUNT
Interim	FROM _____ TO _____	1988 August 31	30

16 SUPPLEMENTARY NOTATION

17 COSATI CODES			18 SUBJECT TERMS (Continue on reverse if necessary and identify by block number)
FIELD	GROUP	SUB-GROUP	X-Ray spectroscopy Laser-produced plasmas

19 ABSTRACT (Continue on reverse if necessary and identify by block number)

High intensity, frequency-tripled, focused light from a multibeam laser system (OMEGA) was utilized to generate plasma of highly-ionized atoms. This work involves the accurate wavelength measurements of 2p-3d,3s,4d,4s lines in L-series spectra of transition elements. The data were collected with high-resolution x-ray spectrographs. The observed lines were classified based on ab initio, atomic structure calculations using adjusted Slater parameters. The spectral results are presented as isoelectronic sequences of the observed and calculated wavelengths for the Li-, Be-, and B-like stages of ionization from atomic numbers 22 (Ti) through 32 (Ge).

20 DISTRIBUTION / AVAILABILITY OF ABSTRACT ☒ UNCLASSIFIED/UNLIMITED ☐ SAME AS RPT ☐ DTIC USERS	21 ABSTRACT SECURITY CLASSIFICATION UNCLASSIFIED
22a NAME OF RESPONSIBLE INDIVIDUAL P. G. Burkhalter	22b TELEPHONE (Include Area Code) (202) 767-2154 22c OFFICE SYMBOL Code 4681

DD Form 1473, JUN 86 Previous editions are obsolete SECURITY CLASSIFICATION OF THIS PAGE

S/N 0102-LF-014-6603

CONTENTS

X-RAY SPECTROSCOPY OF LASER-PRODUCED L-SERIES LINES

INTRODUCTION

Wavelength measurements of L-series x-ray lines have been reported for the past decade. Spectral patterns have been generated using focused laser beams to irradiate targets of most of the transition metals. The Li-like sequence has been pursued from K through Fe [1-3] and more recently for Cu.[4] A number of groups have reported wavelengths for Be-like lines.[5-8] The identifications reported for B-like transitions are more sparse.[7,9] Our work of several years ago made use of the Chroma laser at KMS Fusion, Inc. to generate plasmas in mass-limited targets[10-11] for L-series wavelength measurements. High resolution X-ray spectroscopy was preformed for selected spectral regions with specific elements for line calibrations. The wavelengths of Be-like transitions for Cr through Co in the 5-15 Å region were measured with an accuracy of ±2 mÅ. The objective of that work was to identify L-series line coincidences for photopumping K-series lines of low atomic number gases such as fluorine or neon. We now rely in part on these wavelengths for calibration and identifications in the present spectral data collected with the 24 beam OMEGA laser system at the Laboratory for Laser Energetics, University of Rochester. To extend the isoelectronic sequences, we also determined wavelengths from Ti spectral data collected a few years ago on the N.R.L. Pharos laser system with a high-resolution, 3m grazing incidence spectrograph, designed and constructed at the Goddard Space Flight Center for rocket-borne solar observations and now in use on the OMEGA chamber.[12]

In the present work, we are making systematic identifications by the comparison of measured and predicted wavelengths of the Li-, Be-, and B-like isoelectronic sequences for L-series lines from Ti through Ge.

Manuscript approved July 1, 1988.

EXPERIMENTAL

Cu and Fe spectral data were collected from small diameter spherical targets with a diffraction - crystal spectrograph. This spectrograph, shown in Fig. 1, gives spectral wavelength coverage over 6-16 Å with a curved mica (2d = 19.64 Å) crystal.[13] Spectrograms were collected for Fe, Cu and Al targets using 23 beams of the OMEGA laser system. The spectra were recorded on the film using a moveable slit in front of the spectrograph to record subsequent shots. The spectral data was recorded on Kodak direct exposure film (DEF) whose exposure-density calibrations were previously been determined.[14] The X-ray spectral strips were scanned with a Joyce Loebl densitometer and the line positions were read with a Grant comparator densitometer. The Fe and Cu plasma emissions were generated with frequency - tripled blue light (0.35 μm) operating at 1.1 kJ in 344 psec pulses. The irradiance level was 6.0 x 10^{15} W/cm^2. The targets consisted of coatings of 1 μm thickness on 150 μm diameter, thin-walled plastic spheres supported by a glass stalk. The Si K-series lines from the plasma generated in the supporting glass stalk provided valuable calibration lines.

The Ge plasma was generated using solid microspheres about 400 μm diameter. The OMEGA laser was operated at 1.4 kJ with 24 beams of blue light in 650 psec pulse durations. The irradiance was 3.0 x 10^{15} W/cm^2 for the Ge targets. The Ge spectral lines were calibrated in the 4-10 Å region with the Si K- series lines and the 2p-3d,3s transitions Ne- and F-like Ge.[15]

A Ti spectrum was acquired with the NRL Nd: glass Pharos laser operating at 20 J and 900 psec pulses. The laser beam was focused onto slab targets for an irradiance of 2.0 x 10^{14} W/cm^2. The spectral lines for the other transition elements in the isoelectronic sequences were previous spectral measurements in the 6-18 Å region using the Chroma laser system operated at 20 J in 120 psec pulses. The targets were deposited microdots centered on a

thin Formvar film supported by a washer. Green light (0.527 μm) was used at an irradiance of 1.5×10^{14} W/cm^2. An accuracy of 2 mÅ was achieved by judicious selection of appropriate calibration spectra for the limited spectral regions of interest and the use of high-resolution, flat diffraction crystals. The 2p-3d,3s Be-like Fe transitions were accurately measured in the 11-12 Å region.[11] These wavelength values were used together with wavelengths for first order Al and Si K-lines to calibration the Cu spectra. Identification of Li-, Be-, B-like Cu lines were made in the 6-10 Å region.

Ab initio atomic structure calculations were preformed for comparison of the observed spectral patterns. The good agreement in the predicted and observed wavelengths and spectral patterns allowed line classifications to be made for the Ti, Fe, Cu, and Ge data. Calculations were generated for all the elements from atomic number 20 (Ca) through 32 (Ge) in order to systematically follow the isoelectronic sequences in the three ionization stages.

RESULTS

Spectral data for Fe and Cu were collected on subsequent shots on OMEGA along with Al calibration lines. These spectra were recorded juxtapositioned on the same film. The line positions were read for the Fe and Cu L-series and Al and Si K-series transitions. The Fe spectrum was calibrated with Be-like 2p-3d transition in the 11-12 Å region that have been accurately measured in prior work together with the first order K-series calibration spectral lines. The precision for the line position and wavelength determinations was 1.9 mÅ over the 6-13 Å region. The iron L-series lines in the 8.5-10.0 Å region were compared to reported 2p-3d transitions in F-like Fe XVIII wavelengths[16,17] and the 2p-3s,3d Ne-like Fe XVII lines.[3,15] The agreement was ±5 mÅ for all the measured wavelengths. The Li-like Fe XXIV lines occur in the 8-11.5 Å region for 2p-3s,3d,4d and 2s-3p,4p transitions. The $2s2p^2$-2s2p3d B-like transitions in Fe XXII were identified in the 11.5-12.5 Å region from previous

observations and with the atomic structure predictions by matching observed and calculated wavelengths and recorded film densities with calculated weighted oscillator strengths (gf-values).

The spectrum for Cu plasma emission in OMEGA between 6-12 Å is shown in Fig. 2. The atomic structure calculations are plotted as vertical lines for a few of the intense transitions in Li- and Be-like Cu. These intense lines occur near 9 Å while weak Ne-like 2p-3d lines are found near 11.5 Å. The Cu spectrum was calibrated with Al and Si K-series lines and the Li- and Be-like Fe lines. The precision of wavelength measurement was 1.9 mÅ. The accuracy of the Cu wavelengths is ±5 mÅ when compared to reported Li- and Be-like line values[4] and computed wavelengths for these and B-like lines.

The Ge spectrum is shown in Fig. 3 for the 6-10 Å region. Dominant lines in the spectrum are the 2p-3s,3d transitions in Ne-like Ge XXIII between 9 and 10 Å. The Li-, Be-, and B-like transitions were identified in the 6-8 Å region with the aid of the atomic structure calculations. The observed wavelengths were determined using Al K-series lines and published values for 2p-3s,3d transitions in F-like Ge XXIV [17,18] and Ne-like Ge XXIII.[15,19] The Ge lines were slightly broader than from Fe and Cu data because larger (400 μm diameter) targets were used. The line positions and wavelengths were determined with a fitting precision of 2.4 mÅ and the wavelength accuracy was believed to be ±10 mÅ.

The Ti spectrum was acquired on Kodak 101-5 plate emulsions in the 3m grazing incidence spectrograph at an angle of incidence of 88°. The grating was ruled with 1200 lines/mm, yielding a plate factor in first order of 0.37 Å/mm. The region covered was 10-190 Å; however, the data of interest in this work was 11-19 Å. Calibration was achieved with target impurity lines from O VII and O VIII and from the He alpha line in Na X at 11.003 Å. The lines were read with the Grant comparator densitometer and wavelengths measured with a

precision of 0.8 mÅ. The accuracy was determined to be ±5 mÅ based on agreement with other oxygen lines than those used for calibration.

In the Be-like isoelectronic sequence, two groups of spectral lines were identified and classified. The 2s2p-2s3d and $2p^2$-2p3d transitions for Ti XIX in the 16.4-17.2 Å region are listed in Table 1. The theoretical wavelengths were calculated for Ti XIX using the scaled Slater parameters determined by least-squares fitting in prior work for Cr XXI.[9] The calculated transitions with gf-values greater than 0.3 are listed in the table. All the predicted lines except two (wavelengths at 16.535 and 16.955 Å) were observed in the Ti spectrum. The experimental wavelengths measured for Be-like Ti were in near agreement with the wavelengths measured in previous work involving spectral data collected on the Chroma laser. Line number 15 is an exception as the value we reported previously for the ^1S-^1P line was 17.215 Å, not in agreement with the predicted wavelength of 17.192 Å. In the current data, the predicted and observed spectral wavelengths agree except for line 15 which has a 12 mÅ difference from the predicted value.

The Be-like 2p-3d transitions were calculated for the entire range of ionization stages from Ca XVII through Ge XXIX. These were plotted as wavenumber differences from a dominant spectral line. Figure 4 shows the calculated values (solid line) for the 2s2p-2s3d transitions and Fig. 5 for the $2p^2$-2p3d transitions together with our observed wavenumber values. The data points are numbered to correspond to values in the tables for Be-like Ti XIX, Cu XXVI, and Ge XXIX ionization stages. The difference plots are sensitive to the wavelength classification accuracy. For the lines plotted all the classifications extend over the entire range of ionization stages. The experimental and predicted wavelengths are seen to satisfactorily follow the isoelectronic sequences for the current and prior wavenumber values. The Ti, V through Fe, and Cu data were acquired with spectral resolution adequate

to determine many of the lines distinctly in the Be-like series. The resolution was somewhat less for the Ge data. This is indicated by the bar joining the two dots for transition (2) indicating the line width recorded resulting from the larger target diameter. Most of the experimental values follow the isoelectronic line slopes. An exception is line 14 in which the experimental values are nearly level for V through Ge as opposed to the upward slope predicted for the $^1P_1$-$^1D_2$ transition. There is indication in both the Ti XIX and Fe XXIII data that the $^1S_0$-$^1P_1$ line (15) may be two lines that split and diminish at higher ionization stages. The isoelectronic sequence plots are valuable for predicting wavelengths not available experimentally.

In the B-like isoelectronic sequence, some 11-16 distinct lines were measured and classified as the $2s2p^2$-2s2p3d transitions in Ti XVIII, Fe XXII, Cu XXV, and Ge XXVIII ionization stages. The measured and predicted wavelengths are listed in Tables 4-7. As can be observed many lines are resolved in the x-ray spectral data or are unresolved pairs of closely predicted wavelengths. There is generally good agreement between measured and predicted wavelength values for the B-like transitions.

The wavenumber differences from the reference line $^4P_{5/2}$-$(^3P)^4D_{7/2}$ were plotted in Fig. 6 together with the theoretical values. For the most part, the observed lines follow the predicted line slopes; however, unlike the Be-like lines there are several B-like transitions whose classifications change over the range of ionization stages. This results in part because of line overlap and changing line purity in the theoretical classifications. There are three lines that change their purity mix significantly enough to be important in the B-like transitions plotted in Fig. 6. One such line starts out as $^2D_{3/2}$-$(^3P)^2F_{5/2}$ at Ti XVIII (line 14) and later becomes mixed with the stronger $^2P_{3/2}$-$(^1P)^2D_{5/2}$ transition at Fe XXII (line 9). The $^2D_{3/2}$-$(^3P)^2F_{5/2}$ transition was measured in Cu XXV (line 9) and Ge XXVIII (line 9) but the

wavenumbers fall below the plot axis for these cases. Another instance of changing classification mix is the $^4P_{5/2}$-$(^3P)^4P_{5/2}$ (line 5) in Ti XVIII changing to $^4P_{5/2}$-$(^3P)^4D_{5/2}$ (line 4) in Ge XXVIII. Overall there is good agreement between observed and predicted wavenumbers in the B-like isoelectronic sequence. The Slater parameters determined by least-squares fitting to the Cr and Cu spectral data for the B-like $2s2p^2$-2p3d transitions are listed in Table 8. The adjustments for obtaining the good agreement between the observed and predicted wavelengths are within ±5% of unity for the pure ab initio calculations. The exceptions are Zeta3 at 1.27 and G1 at 0.94. Essentially no adjustment was found necessary in the theoretical calculations of the upper and lower average energy levels.

The Li-like 2-3,4 transitions in Ti XX, Fe XXIV, Cu XXVII, and Ge XXX were measured in the spectral data from OMEGA and Pharos laser systems. The measured and predicted wavelengths are listed in Table 9. There is good agreement between the wavelength values. The asterisk beside the 7.164 Å line in Ge indicates an overlap between the weak $2p_{1/2}$-$3s_{1/2}$ and the intense $2p_{3/2}$-$3d_{5/2}$ lines. This same broad line is found to overlap with transitions in the first line classified in Be-like Ge XXIX 2s2p-2s3d.

The line energies for this and the prior spectral data from the Chroma laser system are plotted as a Moseley diagram in Fig. 7. The lines are identified as to transition and listing for Ge XXX in Table 9. The line energies are found to be linear over these ionization stages.

A potential use for the wavelengths measured in this work is the finding of line coincidences for possible photopumping of K-series levels. A search was made by comparing wavelengths for the Ti, Fe, Cu, and Ge data with K-series transitions in N, O, F, and Ne gases. No wavelength matches were found; however, this systematic approach to wavelength measurement and line

classification allows one to interpolate or extrapolate values for other elements along an isoelectronic sequence.

CONCLUSIONS

The predicted and observed wavelengths agree for the Li-, Be-, and B-like isoelectronic sequences for x-ray spectral data collected in the multibeam OMEGA laser system. The complex L-series lines have been classified based on ab initio atomic structure calculations. The line classifications have been unified with spectral data interpreted from three laser systems.

ACKNOWLEDGMENTS

The authors appreciate the support of Jim Knauer and the entire OMEGA staff at LLE and of Bill Watson and Greg Pien in the LLE target for their assistance in mounting our instrumentation. We wish to thank Charley Brown for the use of the Grant comparator densitometer and John Seely, also of the E O. Hulbert Center, for providing the germanium targets used for acquiring spectral data on OMEGA. We are grateful to Uri Feldman and George Doschek for the titanium exposure collected on the Pharos laser. Special thanks to Karrol Hudson for his assistance in the x-ray data acquisition.

This work was supported by the U.S. Department of Energy, Contract No DE-FC08-85DP40200

References

1. S. Goldsmith, U. Feldman, L. Oren, and L. Cohen, "The lithium-like spectral of K XVII through Mn XXIII in the extreme-ultraviolet region," Astrophys J. 174, 209 (1972).

2. E.V. Aglitskii, V.A. Boiko, S A. Pikuz, and A. Ya Faenov, "Identification of the spectra of laser plasmas of lithium like ions of Ti, V, and Cr in the 8.5 - 17 Å range," Sov. J. Quant. Electron. 4, 956 (1975).

3. V.A. Boiko, A. Ya. Faenov, and S.A. Pikuz, "X-ray spectroscopy of multiply-charged ions from laser plasmas," J. Quant. Spectrosc. Radiat. Transfer 19, 11 (1978).

4. C.M. Brown, J.O. Ekberg, U. Feldman, J.F. Seely, M.C. Richardson, F.J. Marshall, and W.E. Behring, "Transitions in lithiumlike Cu 26+ and beryllium like Cu 25+ of interest for x-ray laser research," J. Opt. Soc. Am. B4, 533 (1987).

5. B.C. Fawcett and R.W. Hayes, "Classification of spectra of K, Ca, Sc, Ti, V and Cr and extrapolation of Fe solar flare lines," Mon. Not. R. Astron. Soc. 170, 185 (1975).

6. V.A. Boiko, S.A. Pikuz, U.I. Safronova, and A. Ya Faenov, "Spectra of Be-like ions with nuclear change Z = 22,...,34 from laser-produced plasmas," J. Phys. B10, 1253 (1977).

7. G E. Bromage, R. D. Cowan, B.C. Fawcett, and A. Ridgeley, "Classification of Be I-like and B I-like iron and vanadium spectra from laser-produced plasmas," J. Opt. Soc. Am. 68, 48 (1978).

8. N. Spector, A. Zigler, H. Zmora, and J.L. Schwob, "Cr, Co, and Ni transitions isoelectronic to the Fe XXIV-Fe XVII lines around 11 Å in laser-produced plasma," J. Opt. Soc. Am. 70, 857 (1980).

9. P.G. Burkhalter, G. Charatis, P.D. Rockett, and D. Newman, "X-ray spectra of B- and Be- like chromium in the 13-15 Å region, " J. Opt, Soc. Am. B1, 155 (1984).

10. P.G. Burkhalter, C.Charatis, and P.D. Rockett, "X-ray spectral line coincidences between fluorine K- and transition-metal L-series lines," J. Appl. Phys. 54, 6138 (1983).

11. P.G. Burkhalter, D.A. Newman, C.J. Hailey, P.D. Rockett, G. Charatis, B.J. MacGowan, and D.L. Matthews, "Spectroscopy of L-series transitions for x-ray laser photopumping," J. Opt. Soc. Am. B2, 1894 (1985).

12. W.E Behring, C.M. Brown, U. Feldman, J.F. Seely, F.J. Marshall, and M.C. Richardson, "Grazing incidence technique to obtain spatially-resolved spectra from laser-heated plasmas," submitted to Appl. Optics.

13. P.G. Burkhalter, D.A. Newman, D.L. Rosen, and K. Hudson, "Spectral measurements from laser-produced plasma in OMEGA," Rev. Sci. Instr. 57, 2171 (1986).

14. P.D. Rockett, C.R. Bird, C.J. Hailey, D. Sullivan, D B. Brown, and P.G. Burkhalter, "X-ray calibration of Kodak direct exposure film," Appl. Optics, 24, 2536 (1985).

15. H. Gordon, M.G. Hobby and N.J. Peacock, "Classification of the x-ray spectra of transitions in the Ne, F and O I isoelectronic sequences of the elements from iron to bromine and in the Na I isoelectronic sequence of gallium to bromine," J. Phys. B13, 1985 (1980).

16. U. Feldman, G.A. Doschek, R.D. Cowan, and L. Cohen, "Fluorine isoelectronic sequence," J. Opt. Soc. Am. 63, 1445 (1973).

17. V.A. Boiko, S.A. Pikuz, A.S. Safronova, and A Ya Fayonov, "Transition between 2p-3d and 2p-3s configurations in the spectra of Fe XVIII ions," Opt. Spectroscopy, 44, 498 (1978).

18. P.G. Burkhalter, G.A.Doschek, U. Feldman, and R.D. Cowan, "Laser-produced x-ray spectra of the fluorine isoelectronic sequence for Zn, Ge, and Se," J. Opt. Soc. Am. 67, 741 (1977).

19. P G. Burkhalter, D.J. Nagel, and R.D. Cowan, "Laser-produced L-series x-ray spectra," Phys. Rev. A11, 782 (1975).

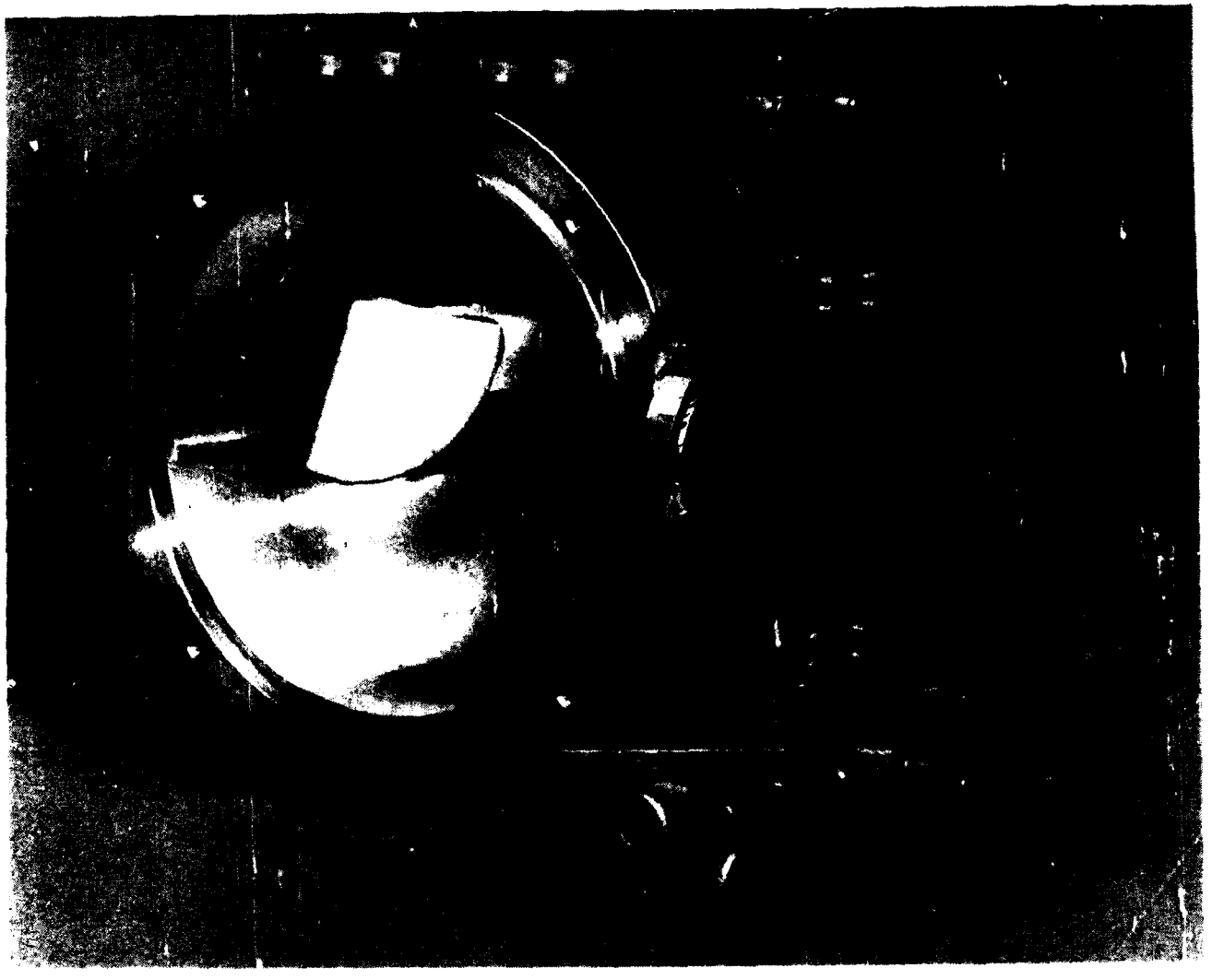

Fig. 1. Photograph of the curved-crystal x-ray spectrograph.

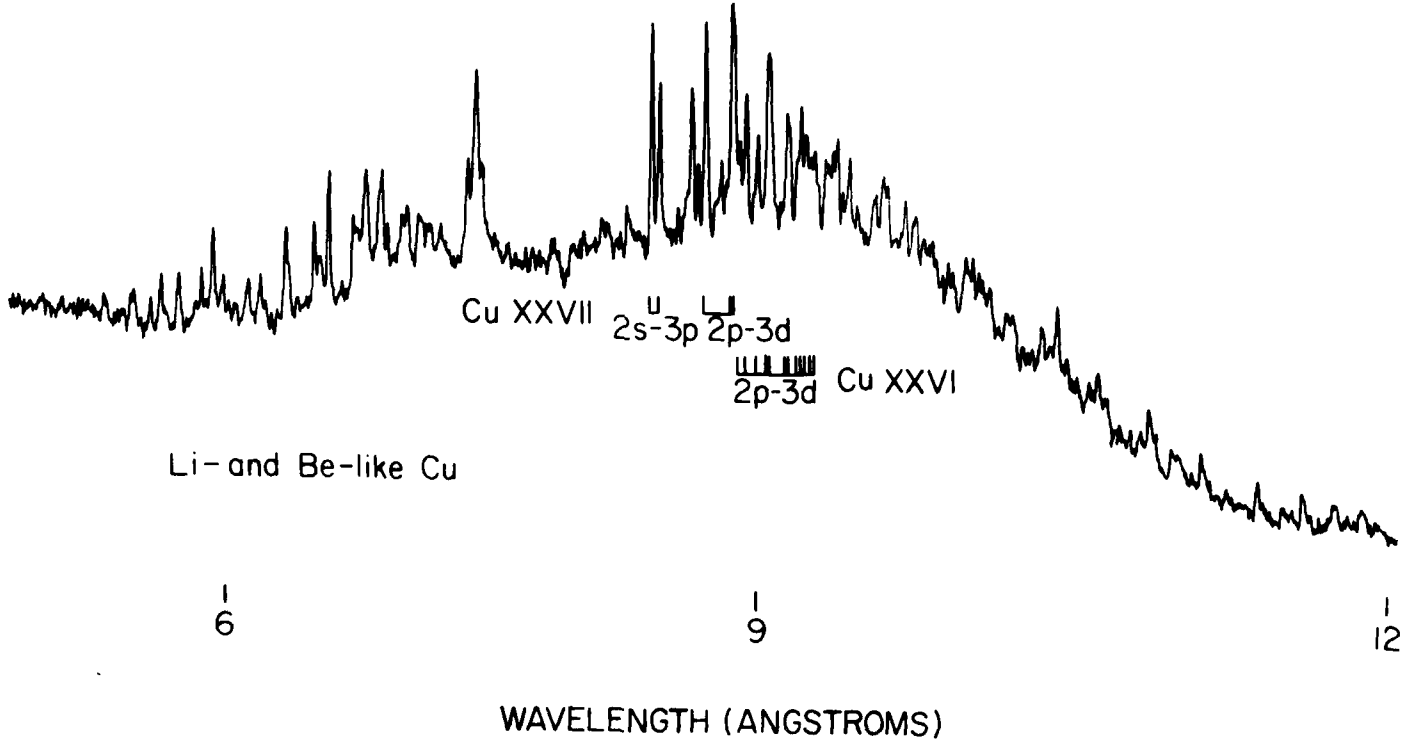

Fig. 2. Cu spectrum identifying some of the Li- and Be-like transitions.

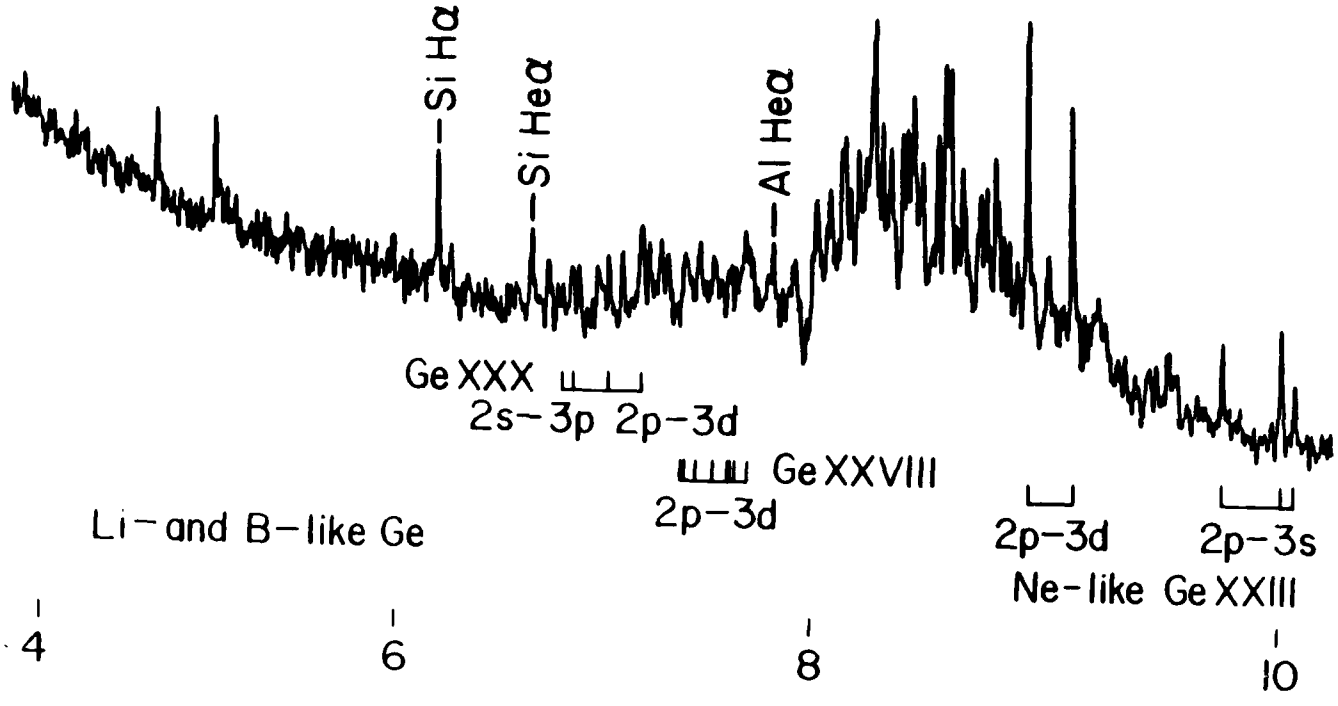

Fig. 3. Ge spectrum collected from OMEGA.

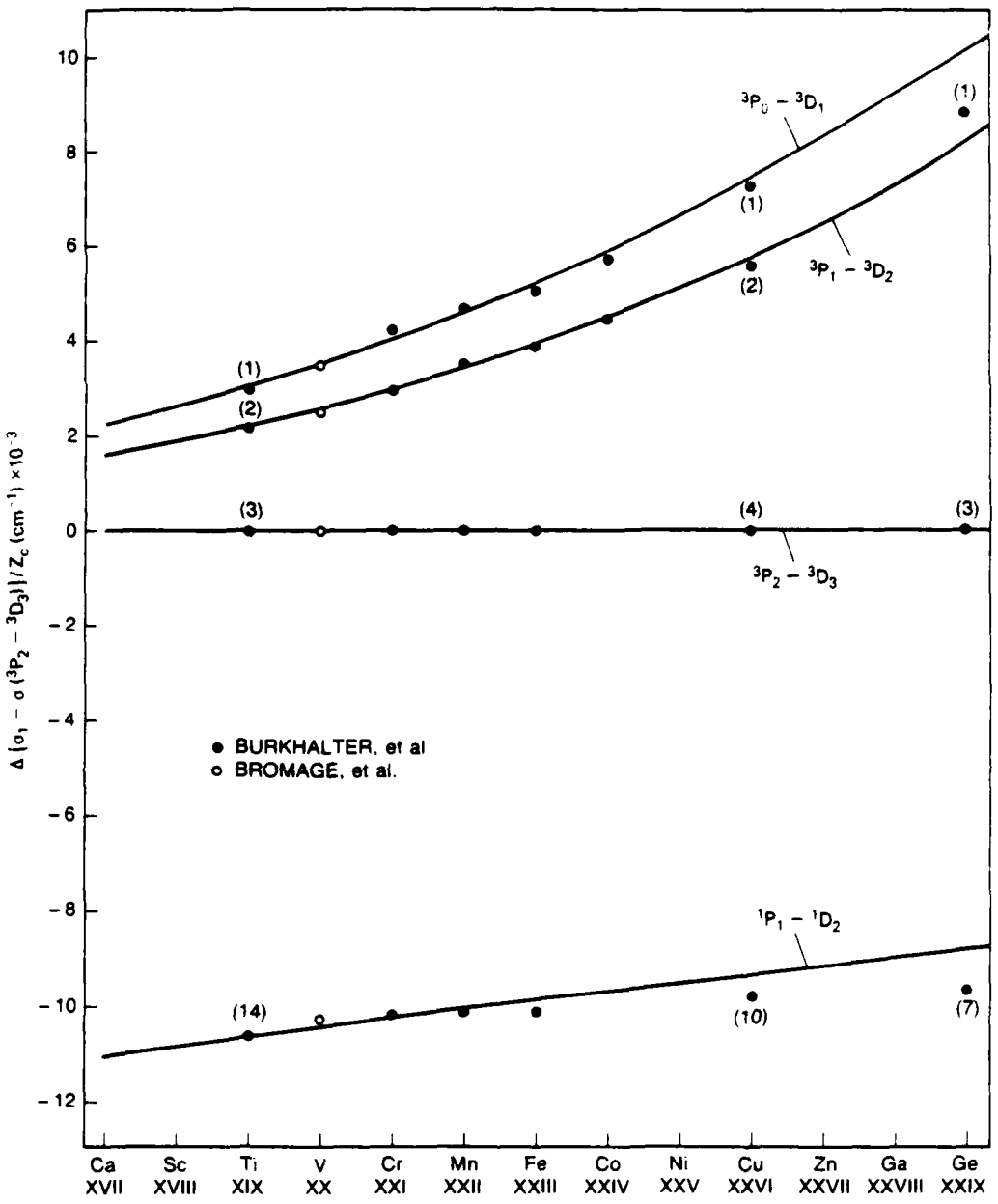

Fig. 4. Be-like isoelectronic sequence. The solid lines are the theoretical wavenumber differences for 2s2p-2s3d transitions. The line numbers for Ti XIX, Cu XXVI and Ge XXIX are listed in Tables 1-3.

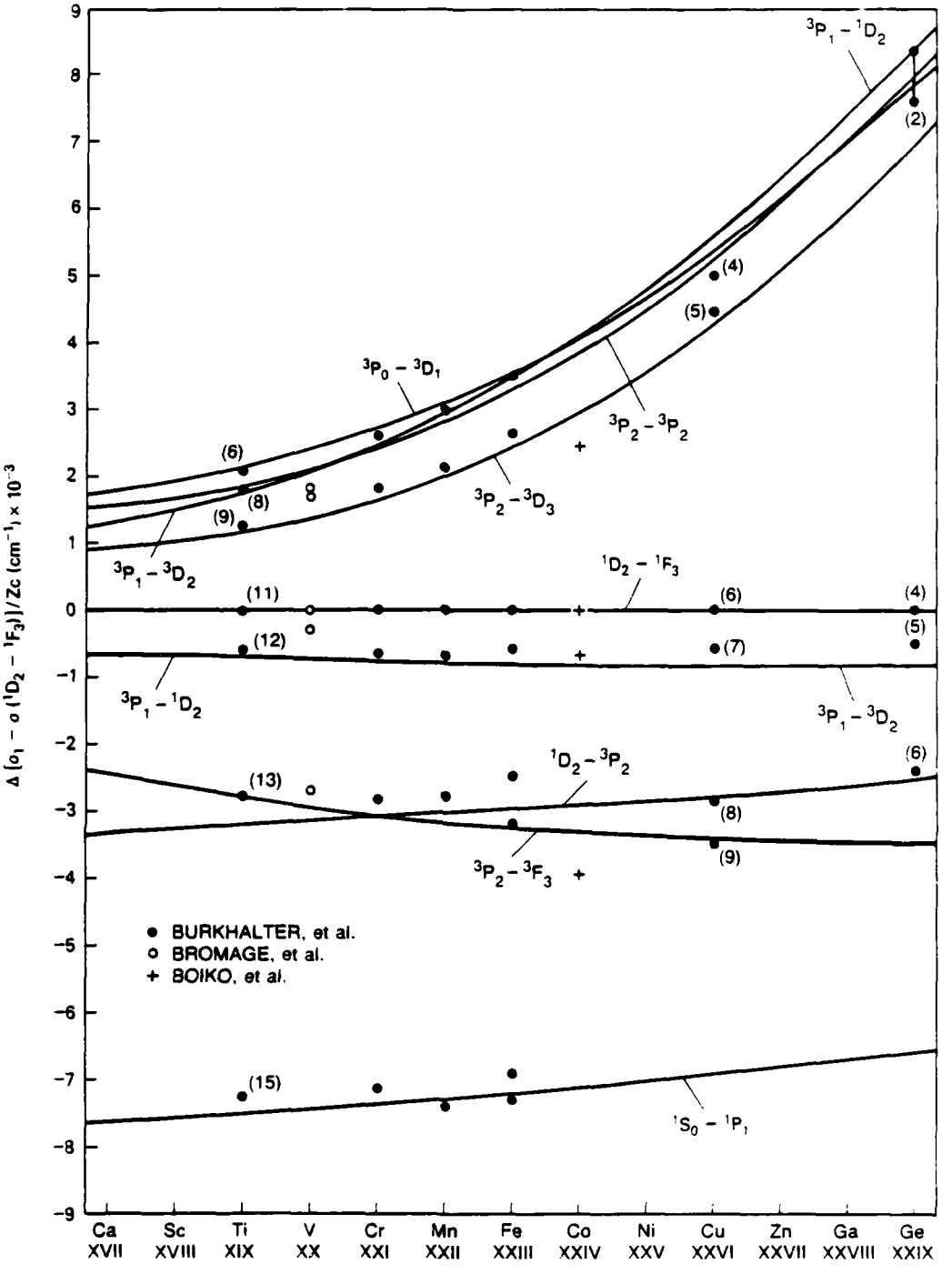

Fig. 5. Be-like isoelectronic sequence for $2p^2$-2p3d transitions.

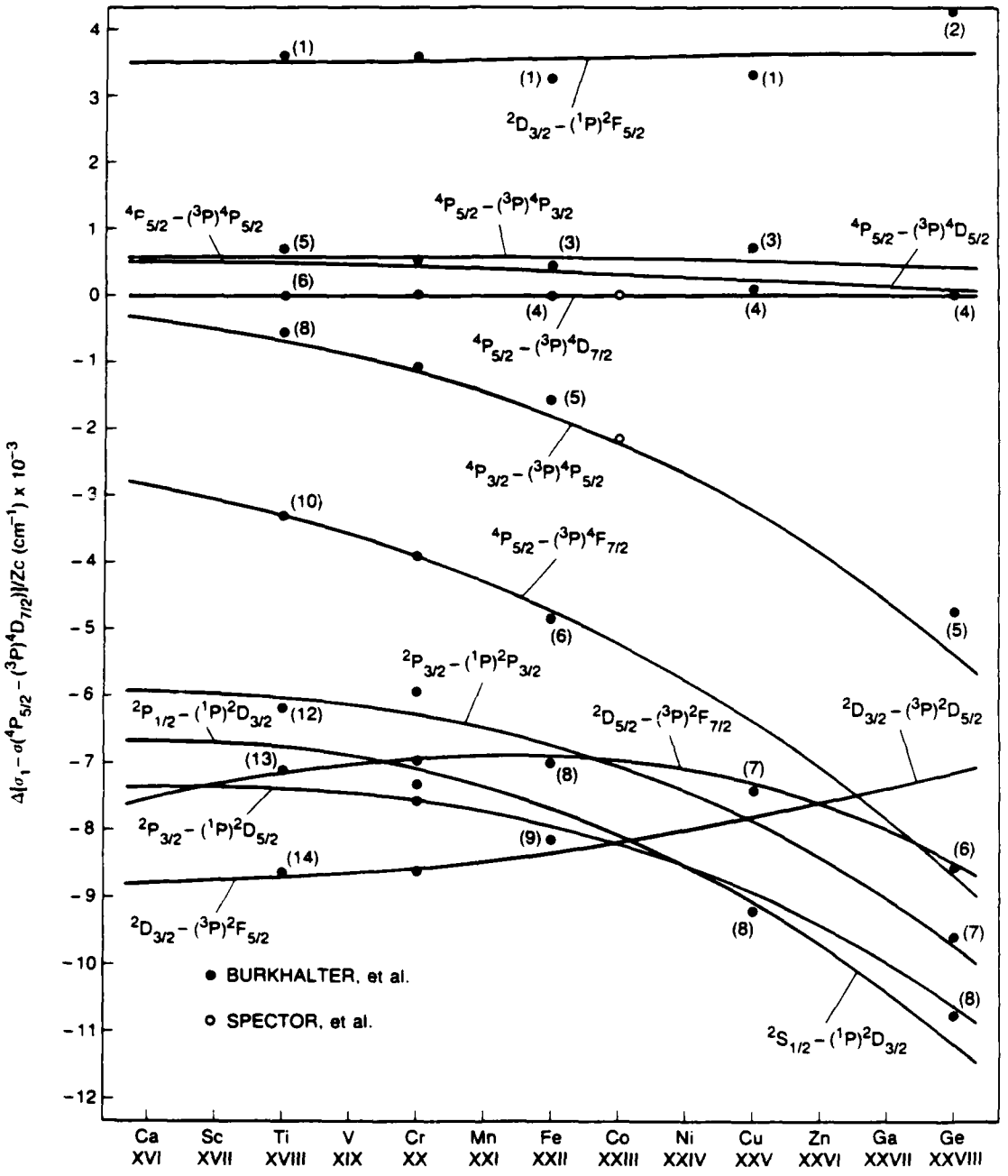

Fig. 6. B-like $2s2p^2$-$2s2p3d$ transitions.

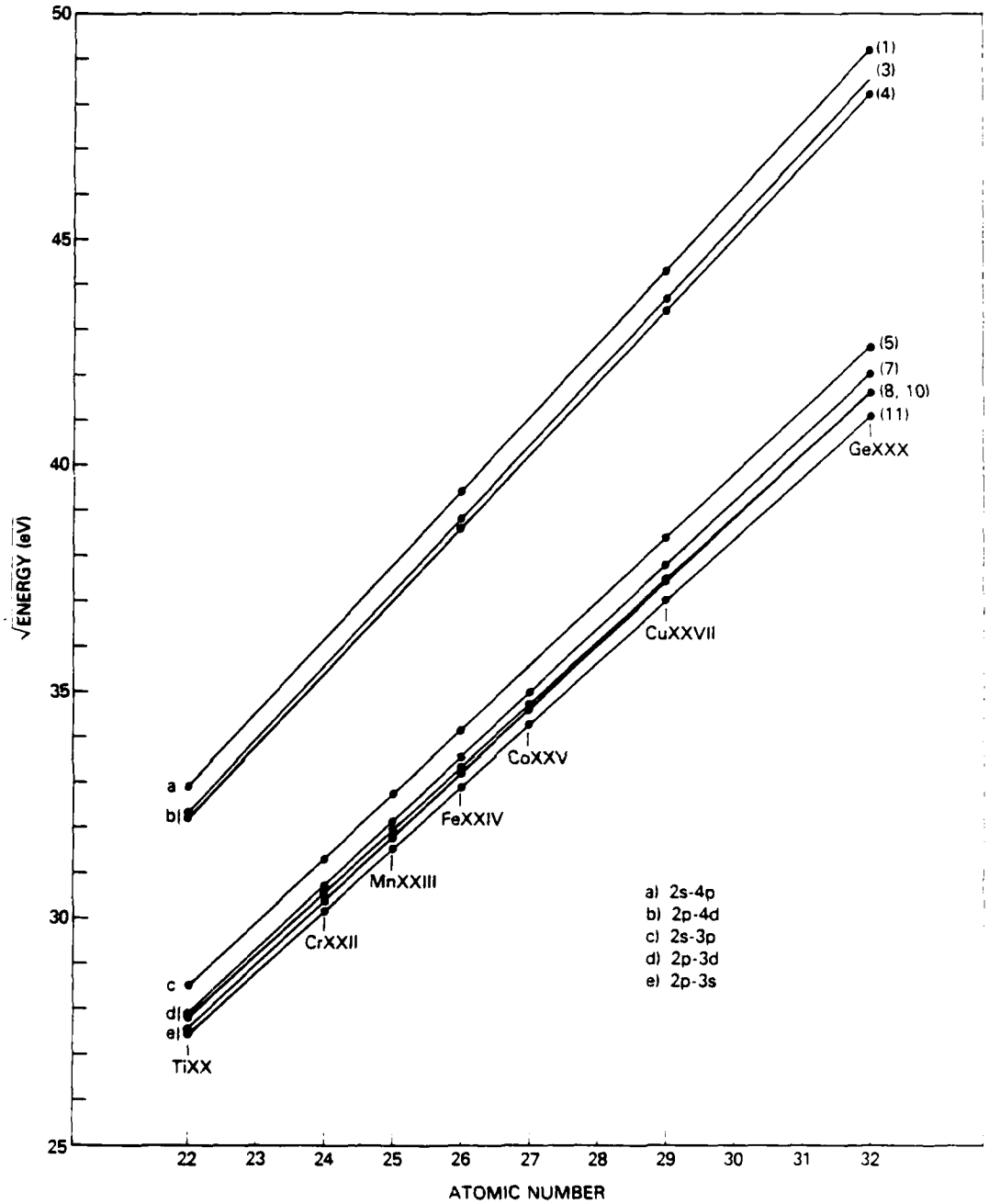

Fig. 7. Moseley diagram for 2-3,4 transitions of Li-like stages of ionization.

Table 1 - Be-Like Ti

Ti Be-like Transitions 2s2p - 2s3d and $2p^2$ - 2p3d

#	Wavelength(Å) Expt.	Calc.	gf	Trans.	Class.
1	16.380	16.379	.67	2s2p - 2s3d	$^3P_0$ - $^3D_1$
2	16.422	16.419	1.5	"	$^3P_1$ - $^3D_2$
		16.424	.50	"	$^3P_1$ - $^3D_1$
3	16.526	16.527	2.8	"	$^3P_2$ - $^3D_3$
		16.535	.50	"	$^3P_2$ - $^3D_2$
4	16.614sh	16.613	.33	$2p^2$ - 2p3d	$^3P_1$ - $^3P_0$
5	16.630	16.620	.68	"	$^3P_1$ - $^3P_1$
6	16.697	16.693	1.3	"	$^3P_0$ - $^3D_1$
7	16.704	16.701	.41	"	$^3P_2$ - $^3P_1$
8	16.710	16.709	1.6	"	$^3P_2$ - $^3P_2$
		16.714	1.6	"	$^3P_1$ - $^3D_2$
9	16.739	16.745	3.6	"	$^3P_2$ - $^3D_3$
10	16.780sh	16.783	.31	"	$^3P_1$ - $^3D_1$
11	16.802	16.802	5.2	"	$^1D_2$ - $^1F_3$
12	16.833	16.838	.93	"	$^3P_1$ - $^1D_2$
13	16.944	16.942	.59	"	$^3P_2$ - $^3F_3$
		16.955	.39	"	$^1D_2$ - $^3P_2$
14	17.064	17.057	1.9	2s2p - 2s3d	$^1P_1$ - $^1D_2$
15	17.180	17.192	1.3	$2p^2$ - 2p3d	$^1S_0$ - $^1P_1$

Table 2 - Be-Like Cu

Cu Be-like Transitions 2s2p - 2s3d and $2p^2$- 2p3d

#	Wavelength(Å) Expt.	Calc.	gf	Trans.	Class.
1	8.879	8.882	.68	2s2p - 2s3d	$^3P_0$ - $^3D_1$
2	8.912	8.914	1.5	"	$^3P_1$ - $^3D_2$
3	8.973	8.973	.77	$2p^2$ - 2p3d	$^3P_1$ - $^3P_1$
4	9.024	9.019	1.3	"	$^3P_0$ - $^3D_1$
		9.022	.87	"	$^3P_2$ - $^3P_2$
		9.029	2.8	2s2p - 2s3d	$^3P_2$ - $^3D_3$
5	9.037	9.041	2.8	$2p^2$ - 2p3d	$^3P_2$ - $^3D_3$
6	9.129	9.130	4.7	"	$^1D_2$ - $^1F_3$
7	9.141sh	9.147	1.6	"	$^3P_1$ - $^3P_2$
8	9.189sh	9.185	1.1	"	$^1D_2$ - $^3P_2$
9	9.201	9.201	1.4	"	$^3P_2$ - $^3F_3$
10	9.228	9.221	1.9	2s2p - 2s3d	$^1P_1$ - $^1D_2$

Table 3 - Be-Like Ge

Ge Be-like Transitions 2s2p - 2s3d and $2p^2$ - 2p3d

#	Wavelength(Å) Expt.	Calc.	gf	Trans.	Class.
1	7.164 b	7.155	.68	2s2p - 2s3d	$^3P_0$ - $^3D_1$
		7.183	1.5	"	$^3P_1$ - $^3D_2$
		7.220	.79	$2p^2$ - 2p3d	$^3P_1$ - $^3P_1$
		7.249	.82	"	$^3P_1$ - $^1D_2$
2	7.263	7.256	.65	"	$^3P_2$ - $^3P_2$
		7.257	1.3	"	$^3P_0$ - $^3D_1$
		7.271	2.6	"	$^3P_2$ - $^3D_3$
3	7.293	7.303	2.8	2s2p - 2s3d	$^3P_2$ - $^3D_3$
4	7.375	7.375	4.6	$2p^2$ - 2p3d	$^1D_2$ - $^1F_3$
5	7.383	7.388	1.6	"	$^3P_1$ - $^3P_2$
6	7.412	7.414	1.3	"	$^1D_2$ - $^3P_2$
		7.428	1.7	"	$^3P_2$ - $^3F_3$
7	7.440	7.437	1.9	2s2p - 2s3d	$^1P_1$ - $^1D_2$
		7.477	1.3	$2p^2$ - 2p3d	$^1S_0$ - $^1P_1$

Table 4 - B-Like Ti

Ti B-like Transitions $2s\ 2p^2$ - $2s\ 2p\ 3d$

#	Wavelength(Å) Expt.	Calc.	gf	Classification
1	17.092	17.093	1.7	$^2D_{3/2}$ - $(^1P)^2F_{5/2}$
2	17.108	17.112	2.0	$^2D_{5/2}$ - $(^1P)^2F_{7/2}$
3	17.149	17.150	.68	$^4P_{3/2}$ - $(^3P)^4P_{1/2}$
		17.153	.85	$^4P_{3/2}$ - $(^3P)^4P_{3/2}$
4	17.215	17.210	1.1	$^4P_{1/2}$ - $(^3P)^4D_{1/2}$
		17.216	1.4	$^4P_{1/2}$ - $(^3P)^4D_{3/2}$
5	17.237	17.238	.67	$^4P_{5/2}$ - $(^3P)^4P_{3/2}$
		17.242	2.0	$^4P_{5/2}$ - $(^3P)^4P_{5/2}$
6	17.272	17.268	4.2	$^4P_{5/2}$ - $(^3P)^4D_{7/2}$
7	17.287	17.286	.46	$^4P_{3/2}$ - $(^3P)^4D_{3/2}$
8	17.300	17.301	1.9	$^4P_{3/2}$ - $(^3P)^4P_{5/2}$
9	17.346	17.353	.49	$^2S_{1/2}$ - $(^1P)^2P_{1/2}$
10	17.441	17.436	.53	$^4P_{5/2}$ - $(^3P)^4F_{7/2}$
11	17.516	17.522	.49	$^2P_{1/2}$ - $(^1P)^2P_{3/2}$
12	17.590 b	17.577	.80	$^2P_{3/2}$ - $(^1P)^2P_{3/2}$
		17.617	1.1	$^2P_{1/2}$ - $(^1P)^2D_{3/2}$
13	17.640 b	17.638	4.1	$^2D_{5/2}$ - $(^3P)^2F_{7/2}$
		17.649	2.9	$^2P_{3/2}$ - $(^1P)^2D_{5/2}$
14	17.721	17.719	1.8	$^2D_{3/2}$ - $(^3P)^2F_{5/2}$
15	17.738	17.738	.57	$^2D_{5/2}$ - $(^3P)^2F_{5/2}$
16	17.991	18.001	.94	$^2S_{1/2}$ - $(^3P)^2P_{3/2}$

Table 5 - B-Like Fe

Fe B-like Transitions $2s\ 2p^2$ - $2s\ 2p\ 3d$

#	Wavelength(Å) Expt.	Calc.	gf	Classification
1	11.742	11.731	1.9	$^2D_{3/2}$ - $(^1P)^2F_{5/2}$
		11.739	.70	$^4P_{3/2}$ - $(^3P)^4P_{1/2}$
		11.741	.95	$^4P_{3/2}$ - $(^3P)^4P_{3/2}$
		11.746	.55	$^4P_{3/2}$ - $(^3P)^4D_{5/2}$
		11.762	1.8	$^2D_{5/2}$ - $(^1P)^2F_{7/2}$
2	11.789	11 789	1.1	$^4P_{1/2}$ - $(^3P)^4D_{1/2}$
		11 794	1.4	$^4P_{1/2}$ - $(^3P)^4D_{3/2}$
3	11.824 *	11.823	2.0	$^4P_{5/2}$ - $(^3P)^4D_{5/2}$
4	11.837	11.834	3.8	$^4P_{5/2}$ - $(^3P)^4D_{7/2}$
		11.848	.52	$^2P_{1/2}$ - $(^1P)^2P_{1/2}$
5	11.883	11.887	1.7	$^4P_{3/2}$ - $(^3P)^4P_{5/2}$
		11.890	.65	$^2P_{1/2}$ - $(^1P)^2D_{3/2}$
6	11.981	11.975	.97	$^4P_{5/2}$ - $(^3P)^4F_{7/2}$
7	12.008	12.005	.58	$^2S_{1/2}$ - $(^1P)^2P_{3/2}$
8	12.046	12.040	4.2	$^2D_{5/2}$ - $(^3P)^2F_{7/2}$
9	12.081	12.072	3.0	$^2P_{3/2}$ - $(^1P)^2D_{5/2}$
		12.084	.85	$^2D_{3/2}$ - $(^3P)^2F_{5/2}$
10	12.102	12.095	.32	$^2P_{3/2}$ - $(^1P)^2D_{3/2}$
		12.119	.95	$^2D_{5/2}$ - $(^3P)^2F_{5/2}$
11	12.203	12.195	1.3	$^2D_{3/2}$ - $(^3P)^2D_{5/2}$
		12.199	.65	$^2P_{1/2}$ - $(^3P)^2P_{3/2}$

* From previous work

Table 6 B-Like Cu

Cu B-like Transitions $2s\ 2p^2$ - $2s\ 2p\ 3d$

#	Wavelength(Å) Expt.	Calc.	gf	Classification
1	9.201	9.190	1.0	$^4P_{3/2}$ - $(^3P)^4P_{3/2}$
		9.196	.75	$^4P_{3/2}$ - $(^3P)^4D_{5/2}$
		9.196	2.0	$^2D_{3/2}$ - $(^1P)^2F_{5/2}$
2	9.228	9.234	1.1	$^4P_{1/2}$ - $(^3P)^4D_{1/2}$
		9.238	1.4	$^4P_{1/2}$ - $(^3P)^4D_{3/2}$
		9.239	1.7	$^2D_{5/2}$ - $(^1P)^2F_{7/2}$
3	9.254	9.259	.53	$^2P_{1/2}$ - $(^3P)^2P_{1/2}$
		9.260	.61	$^4P_{5/2}$ - $(^3P)^4P_{3/2}$
4	9.267	9.265	1.9	$^4P_{5/2}$ - $(^3P)^4D_{5/2}$
		9.270	3.5	$^4P_{5/2}$ - $(^3P)^4D_{7/2}$
5	9.292	9.287	.69	$^2P_{1/2}$ - $(^3P)^2D_{3/2}$
6	9.375	9.375	.47	$^4P_{3/2}$ - $(^3P)^4F_{5/2}$
7	9.424	9.423	4.3	$^2D_{5/2}$ - $(^1P)^2F_{7/2}$
8	9.462	9.458	3.1	$^2P_{3/2}$ - $(^1P)^2D_{5/2}$
		9.461	.78	$^2S_{1/2}$ - $(^1P)^2D_{3/2}$
9	9.540	9.544	1.7	$^2D_{3/2}$ - $(^3P)^2F_{5/2}$
10	9.657	9.654	.76	$^2P_{1/2}$ - $(^3P)^2D_{3/2}$
11	9.696	9.694	.50	$^2P_{1/2}$ - $(^3P)^2P_{3/2}$
12	9.738	9.730	.25	$^2P_{3/2}$ - $(^3P)^2D_{5/2}$

Table 7 - B-Like Ge

Ge B-like Transitions $2s\ 2p^2$ - $2s\ 2p\ 3d$

#	Wavelength(Å) Expt.	Calc.	gf	Classification
1	7.375	7.379	1.0	$^4P_{3/2}$ - $(^3P)^4P_{3/2}$
2	7.384	7.392	2.1	$^2D_{3/2}$ - $(^1P)^2F_{5/2}$
3	7.412	7.418	1.1	$^4P_{1/2}$ - $(^3P)^4D_{1/2}$
		7.440	.56	$^4P_{5/2}$ - $(^3P)^4P_{3/2}$
4	7.446	7.445	1.7	$^4P_{5/2}$ - $(^3P)^4D_{5/2}$
		7.446	3.2	$^4P_{5/2}$ - $(^3P)^4D_{7/2}$
		7.448	1.5	$^2D_{5/2}$ - $(^1P)^2F_{7/2}$
5	7.518	7.527	1.5	$^4P_{3/2}$ - $(^3P)^4P_{5/2}$
		7.554	.16	$^2D_{3/2}$ - $(^3P)^2D_{5/2}$
6	7.576	7.575	4.3	$^2D_{5/2}$ - $(^3P)^2F_{7/2}$
		7.578	1.7	$^4P_{5/2}$ - $(^3P)^4F_{7/2}$
7	7.593	7.594	.74	$^2P_{3/2}$ - $(^1P)^2P_{3/2}$
8	7.612	7.608	3.2	$^2P_{3/2}$ - $(^1P)^2D_{5/2}$
		7.617	1.3	$^2D_{5/2}$ - $(^3P)^2D_{5/2}$
		7.617	.70	$^2S_{1/2}$ - $(^1P)^2D_{3/2}$
9	7.671	7.674	1.8	$^2D_{3/2}$ - $(^3P)^2F_{5/2}$
10	7.776	7.778	.30	$^2P_{3/2}$ - $(^3P)^2P_{3/2}$
11	7.797	7.801	.27	$^2P_{3/2}$ - $(^3P)^2D_{5/2}$

Fig. 8 - Scaling factors used in the atomic structure calculations

Li-like Slater parameter adjustment factors

	$1s^2$ 2s	$1s^2$ 3s	$1s^2$ 2p	$1s^2$ 3p	$1s^2$ 3d	$1s^2$ 4d
EAV	1.0	0.998935	1.0	0.998807	0.999166	0.999256
ZETA 1			0.97	1.0	0.77	0.90

Be-like Slater parameter adjustment factors

$1s^2$ 2s 2p		$1s^2$ 2s 3d		$1s^2$ 2p2		$1s^2$ 2p 3d	
EAV	1.0	EAV	0.9991	EAV	1.0	EAV	1.0
ZETA 2	0.9952	ZETA 2	1.0	F2(11)	0.9389	ZETA 1	1.0090
G1(12)	0.9390	G2(12)	0.9500	ZETA 1	1.0067	ZETA 2	0.9773
						F2(12)	1.0086
						G1(12)	0.9336
						G3(12)	0.7710

B-like Slater parameter adjustment factors

$1s^2$ 2s $2p^2$		$1s^2$ 2s 2p 3d	
EAV	1.0	EAV	0.999932
F2(22)	0.944867	ZETA 2	1.019728
ZETA 2	0.985517	ZETA 3	1.272001
G1(12)	0.950984	F2(23)	0.963803
		G1(12)	0.950352
		G2(13)	0.977243
		G1(23)	0.939709
		G3(23)	0.990547

Fig. 9 - Li-Like transitions in Ti, Fe, Cu, and Ge

Lithiumlike Spectra of Ti, Fe, Cu, and Ge

#	Class.	Ti XX Calc.	Ti XX Expt.	Fe XXIV Calc.	Fe XXIV Expt.	Cu XXVII Calc.	Cu XXVII Expt.	Ge XXX Calc.	Ge XXX Expt.
	2s-4p								
1	$^2S_{1/2}$-$^2P_{3/2}$	11.453	11.448	7.987	7.990	6.319	6.320	5.118	
2	$^2S_{1/2}$-$^2P_{1/2}$	11.463		7.998		6.329		5.128	
	2p-4d								
3	$^2P_{1/2}$-$^2D_{3/2}$	11.871	11.872	8.233	8.230	6.492	6.490	5.245	
4	$^2P_{3/2}$-$^2D_{5/2}$	11.954	11.957	8.316	8.316	6.575	6.575	5.328	5.316
	2s-3p								
5	$^2S_{1/2}$-$^2P_{3/2}$	15.210	15.214	10.621	10.616	8.405	8.402	6.807	6.800
6	$^2S_{1/2}$-$^2P_{1/2}$	15.253	15.257	10.664	10.658	8.449	8.445	6.851	6.842
	2p-3d								
7	$^2P_{1/2}$-$^2D_{3/2}$	15.911	15.914	11.031	11.028	8.695	8.693	7.020	7.015
8	$^2P_{3/2}$-$^2D_{5/2}$	16.054	16.058	11.174	11.175	8.838	8.837	7.164	7.164*
9	$^2P_{3/2}$-$^2D_{3/2}$	16.065	16.071	11.186		8.850	8.848	7.176	
	2p-3s								
10	$^2P_{1/2}$-$^2S_{1/2}$	16.284	16.285	11.270		8.878	8.879	7.167	7.164*
11	$^2P_{3/2}$-$^2S_{1/2}$	16.446	16.444	11.432	11.439	9.040	9.037	7.330	7.342sh